

Available online at www.sciencedirect.com

jmr&t
Journal of Materials Research and Technology
journal homepage: www.elsevier.com/locate/jmrt



Original Article

Evolution of iron-rich intermetallics and its effect on the mechanical properties of Al–Cu–Mn–Fe–Si alloys after thermal exposure and high-temperature tensile testing



Lin Bo ^{a,*}, He Xiangxiang ^a, Xu Rui ^{a,b}, Zhao Yuliang ^c, Lu Yemao ^{b,**},
Xiao Huaqiang ^a

^a School of Mechanical Engineering, Guizhou University, Guiyang, 550025, People's Republic of China

^b Institute of Nanotechnology (INT), Karlsruhe Institute of Technology (KIT), Karlsruhe, 76021, Germany

^c School of Mechanical Engineering, Dongguan University of Technology, Dongguan, 523808, People's Republic of China

ARTICLE INFO

Article history:

Received 20 October 2022

Accepted 24 January 2023

Available online 28 January 2023

Keywords:

Aluminum-copper alloy

High impurity content

Solid-state transformation

High-temperature mechanical properties

ABSTRACT

Si addition is commonly used to modify the iron-rich intermetallics in Al–Cu–Mn–Fe alloys, which is beneficial to increasing the use of recycled aluminum. Most of the available research has focused on the effect of Si content on the room-temperature mechanical properties of Al–Cu–Mn–Fe alloys. To expand the application of Al–Cu–Mn–Fe–Si alloys as light heat-resistant structural components in the automotive and aerospace industries, it is of great importance to investigate the evolution of iron-rich intermetallics and its effect on the fracture behavior of Al–Cu–Mn–Fe–Si alloys after thermal exposure and high-temperature tensile testing. In this work, the evolution of iron-rich intermetallics and the high-temperature mechanical properties of heat-treated Al-6.5Cu-0.6Mn-0.5Fe alloys with different Si contents after thermal exposure and high-temperature tensile testing were assessed by tensile tests, image analysis, scanning electron microscopy, X-Ray diffraction, transmission electron microscopy, and atomic probe tomography. The results indicate that the Al-6.5Cu-0.6Mn-0.5Fe alloys with 0.1Si and 0.5Si additions have excellent and stable high-temperature mechanical properties after long thermal exposure, which are better than those of most heat-resistant Al alloys. The high performance of the high-temperature mechanical properties is attributed to the high heat resistance of secondary intermetallics and precipitated particles. The addition of Si is detrimental to the strength of Al-6.5Cu-0.6Mn-0.5Fe alloys after long thermal exposure. This can be attributed to the solid-state phase transformation of iron-rich intermetallics from α -Fe to β -Fe, which

* Corresponding author.

** Corresponding author.

E-mail addresses: linbo1234@126.com (L. Bo), Yemao.Lu@partner.kit.edu (L. Yemao).<https://doi.org/10.1016/j.jmrt.2023.01.172>2238-7854/© 2023 The Authors. Published by Elsevier B.V. This is an open access article under the CC BY-NC-ND license (<http://creativecommons.org/licenses/by-nc-nd/4.0/>).

results in the increase of needle-like Fe-rich phases and Si particles, the agglomeration of secondary intermetallics, and the consumption of Al₂Cu phases.

© 2023 The Authors. Published by Elsevier B.V. This is an open access article under the CC BY-NC-ND license (<http://creativecommons.org/licenses/by-nc-nd/4.0/>).

1. Introduction

Al–Cu alloys have been widely used as light heat-resistant structural components in the automotive and aerospace industries due to their low specific weight, higher strength, and heat resistance [1,2]. To obtain heat-resistant Al–Cu alloys with high strength and toughness, the strict control of the Fe and Si contents is required [3]. For instance, the maximum Fe and Si content in 206.0 Al–Cu alloys for general purpose use is usually limited to 0.15% and 0.10%, respectively. For aerospace applications, the Fe and Si content in A206.2 Al–Cu cast alloys needs to be below 0.07% and 0.05%, respectively [4]. Nevertheless, the strict control of the Fe and Si contents in heat-resistant Al–Cu alloys increases their cost and limits their industrial applications. To this end, it is important to develop low cost and thermally stable Al–Cu alloys that function well under elevated temperature conditions.

With the increasing requirements of environmental protection and green manufacturing, the recycling of Al alloys has become an important development direction of the aluminum industry [5]. Recycled Al alloys usually contain high amounts of Fe and Si impurities, which can even accumulate during recycling [6]. Consequently, expanding the acceptable range of the Fe and Si contents in heat-resistant Al–Cu alloys would be beneficial to the higher use of recycled Al alloys. In addition, it has been found that, if Fe is added in some heat-resistant Al alloy systems, thermally stable iron-rich intermetallics can be formed. For instance, Fe has been added in order to increase the high-temperature strength of Al–Cu–Mg–Fe–Ni alloys, such as AA2219 and AA2618 [7,8]. Several studies have suggested that Si has a significant modification effect on the formation of Chinese script Fe-rich intermetallics in Al–Cu–Mn alloys [9–11]. Most of these studies have focused on the effect of Si content on the room-temperature mechanical properties of Al–Cu–Mn–Fe alloys [9–11]. For example, Kamaga et al. investigated the effect of the Si/Fe ratio on the room-temperature mechanical properties of B206 alloys and reported that the best mechanical properties can be obtained when the Fe/Si ratio is as close to 1 as possible [9]. Liu et al. investigated the effect of the Fe and Si contents on the room-temperature mechanical properties of A206 alloys and found that the solid-state transformation of α -Fe to β -Fe (abbreviated hereinafter as α -Fe to β -Fe) deteriorated the mechanical properties of A206 alloys with high Fe and Si contents [10]. Zhao et al. studied the effect of Si content on the evolution of the iron-rich intermetallics in heat-treated Al–Cu–Mn–Fe alloys. They reported that the Si addition promoted the formation of α -Fe (Al₁₅(FeMn)₃(CuSi)₂) and led to the α -Fe remaining thermodynamically stable after T5 heat treatment [11]. In our previous works, the effect of Si on the room temperature mechanical properties on Al–Cu–Mn–Fe

alloys has been studied, and it has been found that the addition of Si maintains the α -Fe stable after T7 heat treatment, and promotes the formation of nano-sized α -Fe in Al–Cu–Mn–Fe alloys, which may be beneficial to improving the mechanical properties at elevated temperatures [12]. Experiments including high-temperature thermal exposure and high-temperature tensile testing of Al alloys are commonly used to mimic the actual heat-resistant service conditions. Thus far, the evolution of iron-rich intermetallics and its effect on the high-temperature mechanical properties of Al–Cu–Mn alloys with high Fe and Si content has rarely been investigated. In this study, the evolution of iron-rich intermetallics and its effect on the mechanical properties of Al–Cu–Mn–Fe alloys with different Si contents are assessed through thermal exposure and elevated temperature tensile tests. After the samples were thermally exposed for different times followed by tensile testing at 300 °C (abbreviated hereinafter as TETT), solid-state transformation of iron-rich intermetallics from α -Fe to β -Fe occurred in Al–Cu–Mn–Fe alloys with high Si content. This study is beneficial to the potential use of recycled Al for the manufacture of light heat-resistant structural components, and provides support to development of low cost and thermally stable Al–Cu alloys with high Fe and Si contents.

2. Materials and methods

Alloys were prepared using commercially available pure Al (99.5%), Al-50% Cu, Al-10% Mn, Al-20%Si, and Al-5% Fe master alloys. The compositions of the alloys were determined using optical emission spectrometry, and the results are listed in Table 1. The melting process has been described in detail in our previous work [12]. The T7 heat treatment condition was used here to stabilize the microstructure and decrease the stress corrosion during elevated temperature service [10]. The samples were then solution-treated at 535 °C for 12 h before being quenched in warm water at 100 °C. The samples were then aged using T7 conditions at 215 °C for 16 h [12]. After T7 heat treatment, the round bars were machined into standard tensile test bars. Subsequently, the tensile test bars were thermally exposed in a heat treatment furnace at 300 °C for different holding times of 0.5 h, 10 h, and 100 h. Then, tensile testing was performed on an MTS CMT5105 standard testing

Table 1 – Chemical composition of the alloys.

Alloys	Cu (%)	Mn (%)	Fe (%)	Si (%)	Al (%)
Al-6.5Cu-0.6Mn-0.5Fe-0.1Si	6.60	0.63	0.50	0.08	92.19
Al-6.5Cu-0.6Mn-0.5Fe-0.5Si	6.48	0.61	0.48	0.51	91.92
Al-6.5Cu-0.6Mn-0.5Fe-1.0Si	6.48	0.61	0.47	1.03	91.41

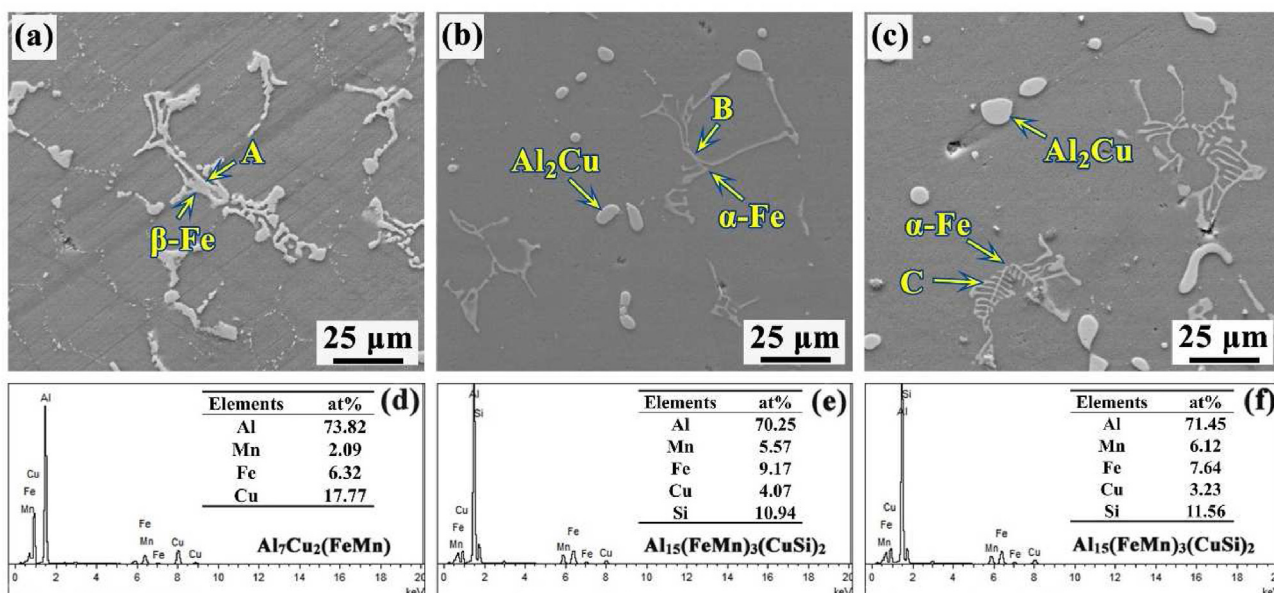


Fig. 1 – Morphology and SEM-EDS mapping of the iron-rich intermetallics in the Al-6.5Cu-0.6Mn-0.5Fe alloys with different Si contents after T7 heat treatment: (a) 0.1Si; (b) 0.5Si; (c) 1.0Si; (d) EDS of point A; (e) EDS of point B; (f) EDS of point C.

machine with a constant temperature box; the reported values were the average values of at least three samples. It should be noted that the thermal exposure and tensile test samples were all tested after T7 heat treatment. The heating rate was 15 °C/min, and the displacement rate was 2.0 mm/min for thermal exposure experiments. Samples for micro-hardness testing and metallographic observation were cut from the gauge length portion of selected tensile specimens. The micro-hardness testing location was controlled within the center of α (Al) dendrite near the center of the etched specimens. The micro-hardness was measured on a micro-hardness tester equipped with a Vickers diamond indenter under an indentation load of 50 g; more than 10 readings were obtained for each sample and the values were averaged. The samples used for metallographic observations were etched for 30 s in a mixture containing 1 mL of HF, 16 mL of HNO₃, 3 g of CrO₃, and 83 mL of H₂O. The iron-rich intermetallics and the fracture surfaces were analyzed using a scanning electron microscope (SEM; Nova Nano SEM 430) with energy dispersive X-ray spectroscopy (EDS). The evolution of the iron-rich intermetallics was analyzed by X-ray diffraction (XRD; Bruker-AXS D8 Advance) with Cu-K_α radiation at a speed of 5°/min and scanning range of 20°–90°. The Transmission samples with a diameter of 3 mm and a thickness of less than 100 μm were taken from the surface layer of the sample, and then ion-milled by an ion-thinning apparatus for finer characterization. Precipitates in the α (Al) matrix were analyzed using a transmission electron microscope (TEM; JEOL JEM-3010) at 200 kV. The Atom probe tomography (APT) samples with dimensions of 0.5 mm × 0.5 mm × 15 mm were prepared by two-step electropolishing, APT measurements were conducted using a Cameca-LEAP 4000 HR instrument in voltage probe mode at 55 K, a pulse rate of 200 kHz, and a target detection rate of 0.5%. The reconstruction of APT data was performed with the AP Suite 6 software.

3. Results

3.1. Microstructure of Al-6.5Cu-0.6Mn-0.5Fe alloys with different Si contents after T7 heat treatment

Fig. 1 depicts the morphology and SEM-EDS mapping of the iron-rich intermetallics in the Al-6.5Cu-0.6Mn-0.5Fe alloys with different Si contents after T7 heat treatment. According to the EDS mapping of point A-C (Fig. 1d–f) the iron-rich intermetallics were all β -Fe (Al₇Cu₂(FeMn)) phases in the 0.1Si alloys (Fig. 1a). The results indicate that the metastable iron-rich intermetallics α -Fe (Al₁₅(FeMn)₃Cu₂) in the 0.1Si alloys changed into stable β -Fe (Al₇Cu₂(FeMn)) phases after T7 heat treatment [13,14]. In the 0.5Si and 1.0Si alloys (Fig. 1b–c), the iron-rich intermetallics were still α -Fe (Al₁₅(FeMn)₃(CuSi)₂), which indicates that the presence of Si maintained the α -Fe stable after T7 heat treatment. In general, α -Fe remains stable and reduces the Cu consumption in alloys with high Si content, which leads to an increase in the Al₂Cu phase at the grain boundaries.

In Fig. 2, the 3-D morphology of the iron-rich intermetallics at the fracture surface of the Al-6.5Cu-0.6Mn-0.5Fe alloys with different Si contents after T7 heat treatment can be observed. In the 0.1Si alloys, the β -Fe (Al₇Cu₂(FeMn)) existed in cylinder-shaped or cluster-like forms (Fig. 2a), which is in accord with the findings of our previous works [15]. In alloys with high Si content, the α -Fe (Al₁₅(FeMn)₃(CuSi)₂) exhibited a dendritic shape (Fig. 2b–c), further proving that α -Fe was stable after T7 heat treatment [12].

3.2. Microstructure of Al-6.5Cu-0.6Mn-0.5Fe alloys with different Si contents after TETT

Fig. 3 shows the morphology and EDS mapping of the iron-rich intermetallics in the Al-6.5Cu-0.6Mn-0.5Fe alloys with high Si

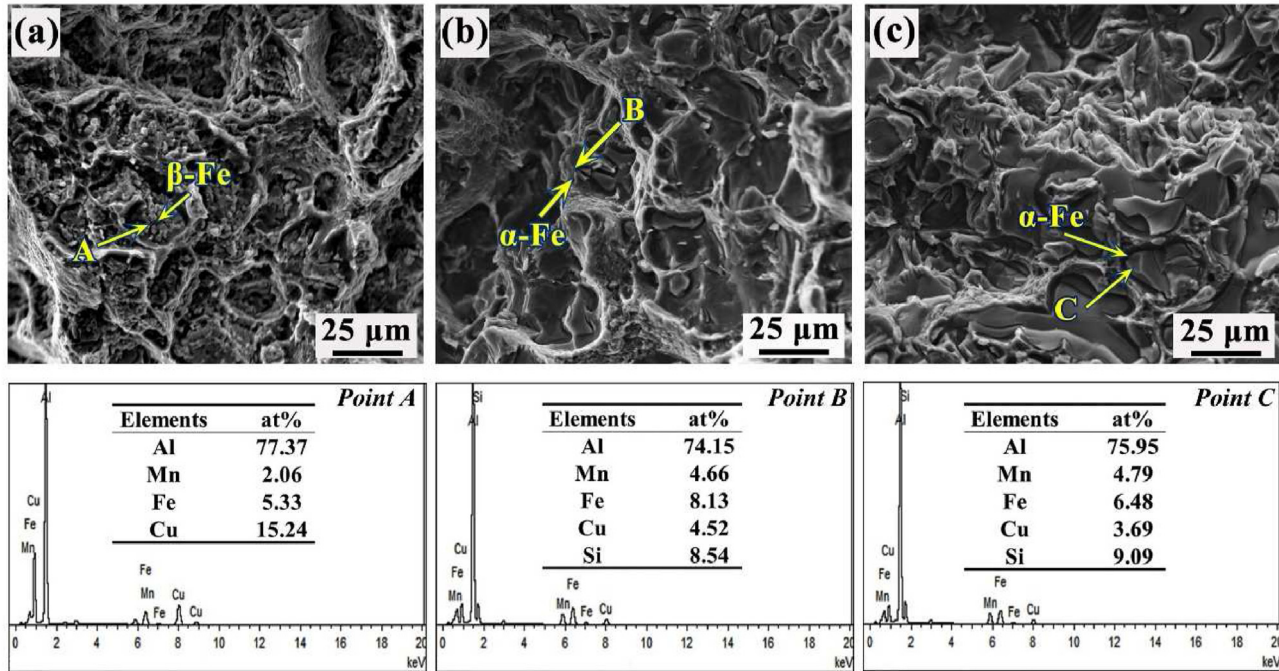
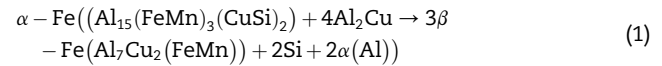


Fig. 2 – 3-D morphology of iron-rich intermetallics in the fracture surfaces of Al-6.5Cu-0.6Mn-0.5Fe alloys with different Si contents after T7 heat treatment: (a) 0.1Si; (b) 0.5Si; (c) 1.0Si.

content after TETT for 100 h. Table 2 shows the EDS data of the iron-rich phases in high-Si-content alloys after TETT for 100 h. It was found that most of the iron-rich intermetallics were Chinese script α -Fe phase. However, a portion of α -Fe was transformed into needle-like β -Fe phase and a small amount of Si particles, which indicates that the α -Fe phases were unstable after TETT for 100 h. The EDS mapping and EDS data of the iron-rich intermetallics revealed that the newly formed β -Fe contained a significant amount of Cu in its chemical compositions. As a result, it can be deduced that the α -Fe to β -

Fe occurred after TETT for 100 h. The solid-state transformation relationship for the iron-rich intermetallics can be expressed as Eq. (1):



From the EDS mapping and EDS data, as well as the solid-state transformation equation, it can be concluded that the solid-state transformation of iron-rich intermetallics from α -Fe to β -Fe, including the formation of needle-like β -Fe, the

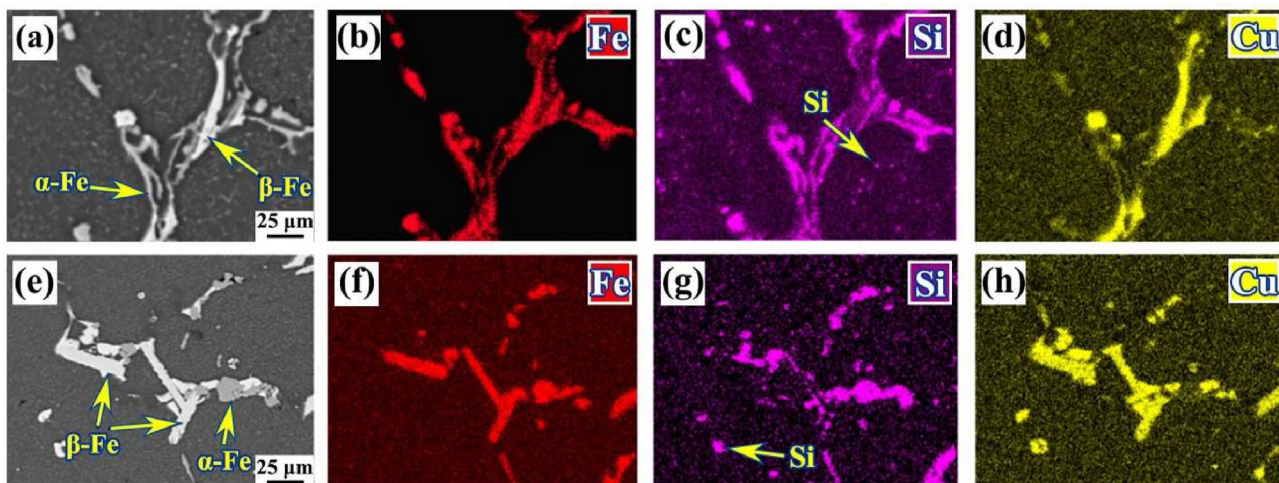


Fig. 3 – Morphology and EDS mapping of iron-rich intermetallics in the Al-6.5Cu-0.6Mn-0.5Fe alloys with different Si contents after TETT for 100 h: (a) microstructure of the 0.5Si alloy; (b) EDS mapping of Fe element; (c) EDS mapping of Si element; (d) EDS mapping of Cu element; (e) microstructure of the 1.0Si alloy; (f) EDS mapping of Fe element; (g) EDS mapping of Si element; (h) EDS mapping of Cu element.

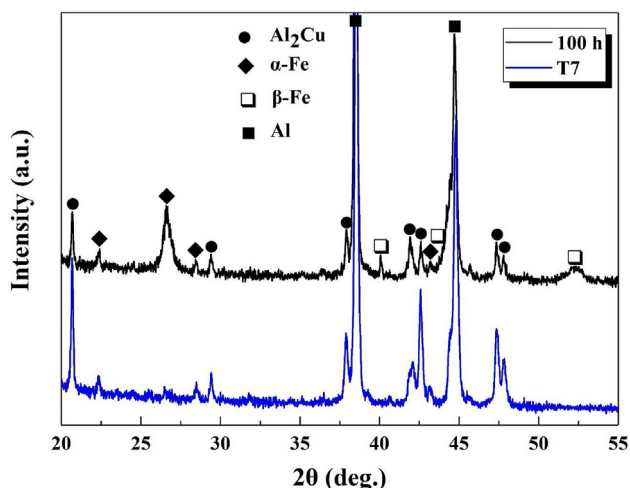
Table 2 – Chemical compositions of the iron-rich intermetallics in high Si content alloys after TETT for 100 h.

Source	Phase	Al (%)	Cu (%)	Mn (%)	Fe (%)	Si (%)
0.5Si	β -Fe	73.82	17.78	2.08	6.32	–
0.5Si	α -Fe	77.71	3.59	3.42	7.00	8.28
1.0Si	α -Fe	77.12	2.90	3.35	7.01	9.62
1.0Si	β -Fe	73.33	18.28	1.96	6.43	–

consumption of Al_2Cu strengthening phases, and the formation of Si particles, may deteriorate the high-temperature mechanical properties of the alloy. In addition, by comparing the microstructures of alloys with different Si content (Fig. 3a and e), it can be found that the increase of the Si content may promote this solid-state transformation of the iron-rich intermetallics from α -Fe to β -Fe significantly.

To further prove the α -Fe to β -Fe, XRD analysis was performed. Fig. 4 reveals the XRD patterns of the Al-6.5Cu-0.6Mn-0.5Fe-1.0Si alloy after T7 heat treatment or TETT for 100 h. The samples treated only with T7 heat-treatment contained Al, Al_2Cu , and α -Fe phases. On the other hand, the samples after TETT for 100 h contained Al, Al_2Cu , α -Fe, and β -Fe phases. The XRD analysis results further proved the α -Fe to β -Fe after T7 heat treatment and TETT for 100 h.

Fig. 5 demonstrates the microstructure of Al-6.5Cu-0.6Mn-0.5Fe alloys with different Si contents after TETT. In the 0.1Si alloy, only Chinese script-like β -Fe was observed, which can be attributed to the full α -Fe to β -Fe after T7 heat treatment (Fig. 5a–c). In addition, the morphology of the Chinese script-like β -Fe remained stable, which indicates the high heat resistance of the β -Fe phases [16]. When the Si content was increased to 0.5% and 1.0% (Fig. 5d–j), the microstructure of the alloys with high Si content contained α -Fe, β -Fe, Al_2Cu , and Si particles, which indicates that the α -Fe phases in high-Si-content alloys are unstable and undergo solid-state phase transformation after TETT. Moreover, with the increase of the thermal exposure time and Si content, the α -Fe to β -Fe

**Fig. 4 – XRD patterns of Al-6.5Cu-0.6Mn-0.5Fe-1.0Si alloy after T7 treated or TETT for 100 h.**

becomes more severe, and the newly formed Si particles agglomerate with the Al_2Cu phases [12].

Fig. 6 and Fig. 7 reveal the precipitated particle morphology, selected electron diffraction patterns, and energy spectrums results of the 0.5Si alloy after TETT for 0.5 h. From Fig. 6, it seems that the SADP results confirm the nano-sized needle shaped like precipitated particles are θ (Al_2Cu) phases (Fig. 6a–c) [1]. The EDS result of the needle shaped like precipitated particles contains Al and Cu elements, further confirms that these phases are θ (Al_2Cu) phases (Fig. 6d). And it finds that the SADP results confirm this rod shaped like precipitated particles are T ($\text{Al}_{20}\text{Cu}_2\text{Mn}_3$) phases (Fig. 6e–g) [17]. The EDS result of the needle shape like precipitated particles contains Al, Cu and Mn elements, further confirming that these phases are T ($\text{Al}_{20}\text{Cu}_2\text{Mn}_3$) phases (Fig. 6h). From Fig. 7, the SADP results confirm the nano-sized cubic shaped like precipitated particles are α -Fe ($\text{Al}_{15}(\text{MnFe})_3(\text{CuSi})_2$) phases (Fig. 7a–b). The EDS result of the needle shaped like precipitated particles contains Al, Cu, Mn, Fe, Si elements, further confirming that these phases are α -Fe ($\text{Al}_{15}(\text{MnFe})_3(\text{CuSi})_2$) phases (Fig. 7c–h) [18].

Fig. 8 presents the precipitated particles of Al-6.5Cu-0.6Mn-0.5Fe alloys with different Si contents after TETT. The size of the precipitated particles was measured using the image J software. In the 0.1Si alloy (Fig. 8a–c), the size of θ (Al_2Cu) was determined to be about 500 nm and that of α -Fe about 200 nm, while no changes were observed with thermal exposure time. In the 0.5Si alloy (Fig. 8d–f), the size of θ (Al_2Cu) was determined to be about 225 nm and that of α -Fe about 88 nm, and nearly no changes were observed with thermal exposure time. In the 1.0Si alloy (Fig. 8g–i), the size of θ (Al_2Cu) was determined to be about 332 nm and that of α -Fe about 106 nm. Besides, the amounts of θ (Al_2Cu) decrease obviously with thermal exposure time in the 1.0Si alloys, which could be attributed to the transformation α -Fe to β -Fe. The size of T ($\text{Al}_{20}\text{Cu}_2\text{Mn}_3$) was measured to range between 0.5 and 2 μm , and exhibited nearly no changes for different thermal exposure times and Si contents. The size of the precipitated particles, including the θ (Al_2Cu), T ($\text{Al}_{20}\text{Cu}_2\text{Mn}_3$), and α -Fe phases, exhibited nearly no changes with increasing thermal exposure time, which indicated the high heat resistance of these precipitated particles. When the Si content increased from 0.1% to 0.5%, the θ (Al_2Cu) and α -Fe phases were significantly refined and the contents of the θ (Al_2Cu) and α -Fe phases increased significantly, while that of T ($\text{Al}_{20}\text{Cu}_2\text{Mn}_3$) decreased slightly. It seems that the addition of Si promotes the formation of θ (Al_2Cu) and α -Fe phases [12,19,20]. Furthermore, it has been found that the Si addition causes the contents of θ (Al_2Cu) to decrease with increasing thermal exposure time.

3.3. Mechanical properties

Fig. 9 illustrates the micro-hardness of the Al-6.5Cu-0.6Mn-0.5Fe alloys with different Si contents after TETT. It was found that the micro-hardness of the Al-6.5Cu-0.6Mn-0.5Fe alloys with different Si contents decreased significantly when the time of TETT was increased from 0.5 h to 100 h. However, the micro-hardness reduction rate increased when the Si content was increased from 0.1 to 1.0, especially for the 1.0Si alloy. After TETT for 0.5 h, the micro-hardness increased

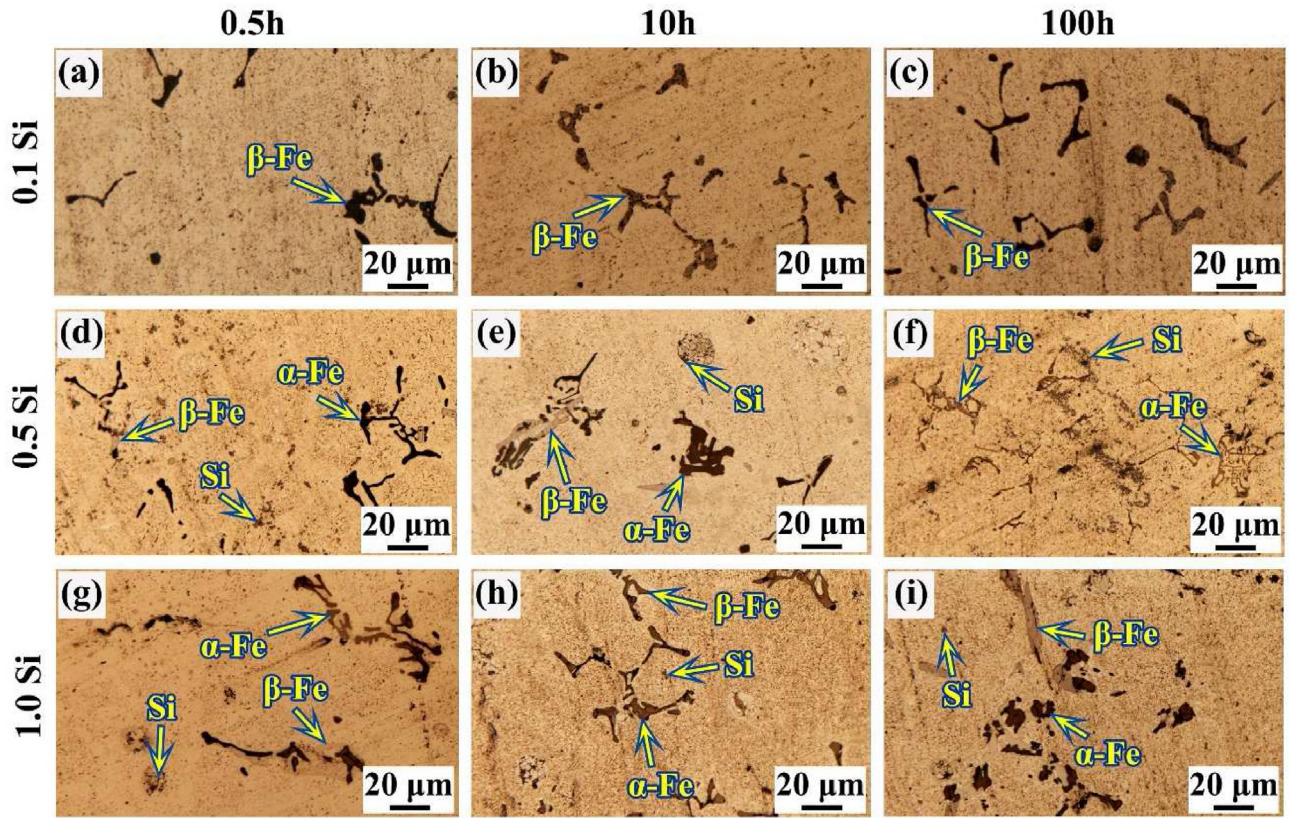


Fig. 5 – Microstructures of Al-6.5Cu-0.6 Mn-0.5 Fe alloys with different Si contents after TETT: (a) 0.1Si, 0.5 h; (b) 0.1Si 10 h; (c) 0.1Si, 100 h; (d) 0.5Si, 0.5 h; (e) 0.5Si, 10 h; (f) 0.5Si, 100 h; (g) 1.0Si, 0.5 h; (h) 1.0Si, 10 h; (i) 1.0Si, 100 h.

from 95.4 HV in the 0.1Si alloy to 111.2 HV in the 1.0Si alloy. The increase of the micro-hardness with increasing Si content can be attributed to the increased content of nano-sized α -Fe and θ (Al_2Cu), as well as to the refinement of the θ (Al_2Cu)

phases [12,19,20]. After TETT for 10 h, the micro-hardness increased from 93.4 HV in the 0.1Si alloy to 97.3 HV in the 0.5Si alloy, while it decreased to 82.7 HV in the 1.0Si alloy. The evolution of micro-hardness can be attributed to the

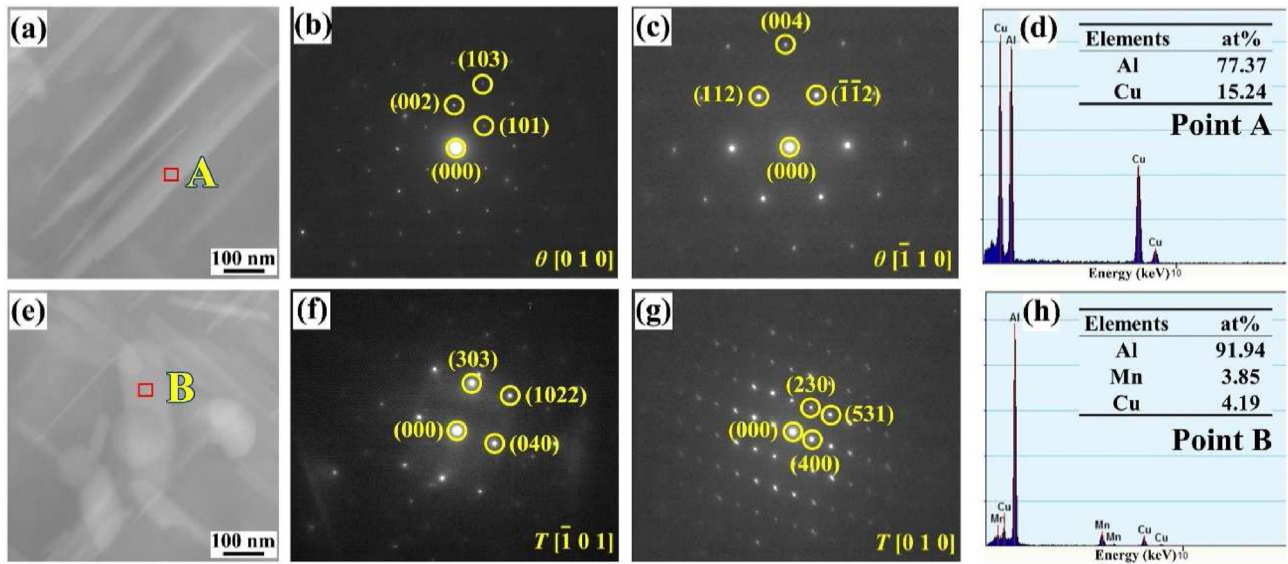


Fig. 6 – Morphology, SADPs, and EDS of θ and T phases: (a) morphology of the θ phase; (b) and (c) the SADP of the θ phase with the zone axis of $[0\ 1\ 0]$ and $[-1\ 1\ 0]$, respectively; (d) the EDS of θ phase; (e) morphology of the T phase; (f) and (g) the SADP of the T phase with the zone axis of $[-1\ 0\ 1]$ and $[0\ 1\ 0]$, respectively; (h) the EDS of T phase.

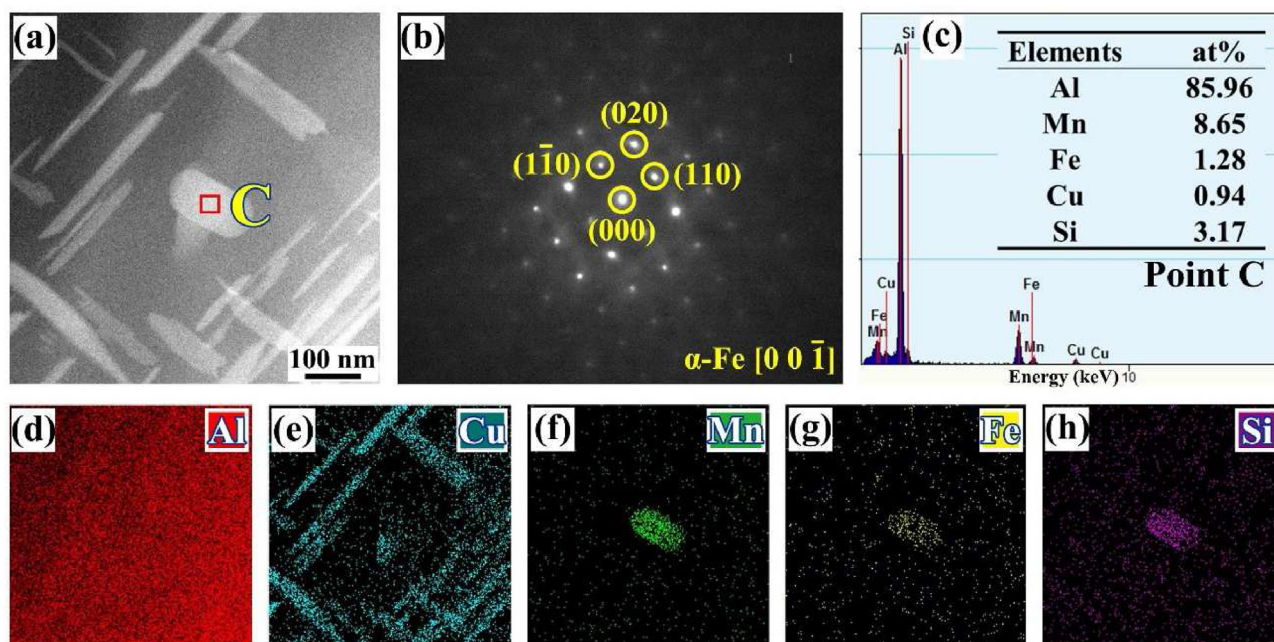


Fig. 7 – Morphology, SADP, and EDS of α -Fe phase: (a) morphology of the α -Fe phase; (b) the SADP of the α -Fe phase with the zone axis of $[0\ 0\ \bar{1}]$; (c) the EDS of the α -Fe phase; (d) EDS mapping of Al element; (e) EDS mapping of Cu element; (f) EDS mapping of Mn element; (g) EDS mapping of Fe element; (h) EDS mapping of Si element.

comprehensive effects caused by the addition of Si, which include the increased content of nano-sized α -Fe and θ (Al_2Cu), as well as the refinement of the θ (Al_2Cu) phase. Moreover, the consumption of the Al_2Cu phases resulted from the solid-state transformation of α -Fe to β -Fe. After TETT for 100 h, the microhardness decreased from 82.9 HV in the 0.1Si alloy to 67.7 HV in the 1.0Si alloy, which can be attributed to the consumption of the Al_2Cu phases due to the solid-state transformation of α -Fe to β -Fe.

Fig. 10 demonstrates the mechanical properties of the Al-6.5Cu-0.6Mn-0.5Fe alloys with different Si contents after TETT. With the increase of the thermal exposure time, the ultimate tensile strength (UTS) and yield strength (YS) (Fig. 10a and b) of the 0.1Si and 0.5Si alloys decreased slightly, and those of the 1.0Si alloy decreased sharply, while the ultimate elongation (EL) (Fig. 10c) of all alloys with different Si contents increased significantly, especially that of the 1.0Si alloys. For example, when TETT for 0.5 h, the UTS decreased from 154 MPa in the 0.1Si alloy to 137 MPa in the 1.0Si alloy, the YS increased from 123 MPa in the 0.1Si alloy to 130 MPa in the 1.0Si alloy, and the EL decreased from 5.0% in the 0.1Si alloy to 3.6% in the 1.0Si alloy. When TETT for 100 h, the UTS decreased from 137 MPa in the 0.1Si alloy to 78 MPa in the 1.0Si alloy, the YS decreased from 108 MPa in the 0.1Si alloy to 70 MPa in the 1.0Si alloy, and the EL increased from 8.3% in the 0.1Si alloy to 11.1% in the 1.0Si alloy.

To evaluate the obtained high-temperature UTS values, the UTS values of experimental alloys with different Si content were compared to those of heat-resistant Al alloys, which are presented in Table 3 [21–29]. The UTS values of the experimental alloys with different Si content were higher than most of the heat-resistant Al alloys, including cast Al–Si alloys, cast

Al–Cu alloys, and the commercial wrought Al alloys. For instance, the UTS values of the Al-6.5Cu-0.6Mn-0.5Fe-0.1Si alloy after TETT for 0.5 h, 10 h, and 100 h were 154 MPa, 140 MPa, and 137 MPa, respectively. The UTS values of the Al-6.5Cu-0.6Mn-0.5Fe-0.1Si alloy were almost two-fold higher than those of commercial wrought Al alloys. It is remarkable that the UTS value of the Al–Si–Cu–Mn–Fe alloy after TETT for 0.5 h was close to that of the Al-6.5Cu-0.6Mn-0.5Fe-0.1Si alloy; however, the UTS values of the Al–Si–Cu–Mn–Fe alloy after TETT for 10 h and 100 h were far lower than those of the Al-6.5Cu-0.6Mn-0.5Fe-0.1Si alloy, and even lower than those of the Al-6.5Cu-0.6Mn-0.5Fe-0.5Si alloy. Although the UTS values of the experimental alloys developed in this study decreased significantly with increasing Si content, especially when the time of TETT was increased to 100 h, the UTS values of the Al-6.5Cu-0.6Mn-0.5Fe-1.0Si alloys after TETT for 0.5 h, 10 h, and 100 h were 137 MPa, 110 MPa, and 78 MPa, respectively. The UTS values of the Al-6.5Cu-0.6Mn-0.5Fe-1.0Si alloys were higher than or close to those of commercial Al alloys.

3.4. Fracture surface characterization

Fig. 11 shows the fracture surfaces of Al-6.5Cu-0.6Mn-0.5Fe alloys with different Si content after TETT. Several dimples and tearing ridges were observed in the fracture surfaces of all alloys, which indicated that the Al-6.5Cu-0.6Mn-0.5Fe alloys with different Si content present ductile fracture characteristics. When the thermal exposure time was increased, the ductile fracture characteristics became slightly less apparent in the 0.1Si alloy, indicating a more stable microstructure (Fig. 11a–c). Cylinder-shaped or cluster-like β -Fe ($\text{Al}_7\text{Cu}_2(\text{FeMn})$) was found in the fracture surfaces of the 0.1Si alloy. In general, the

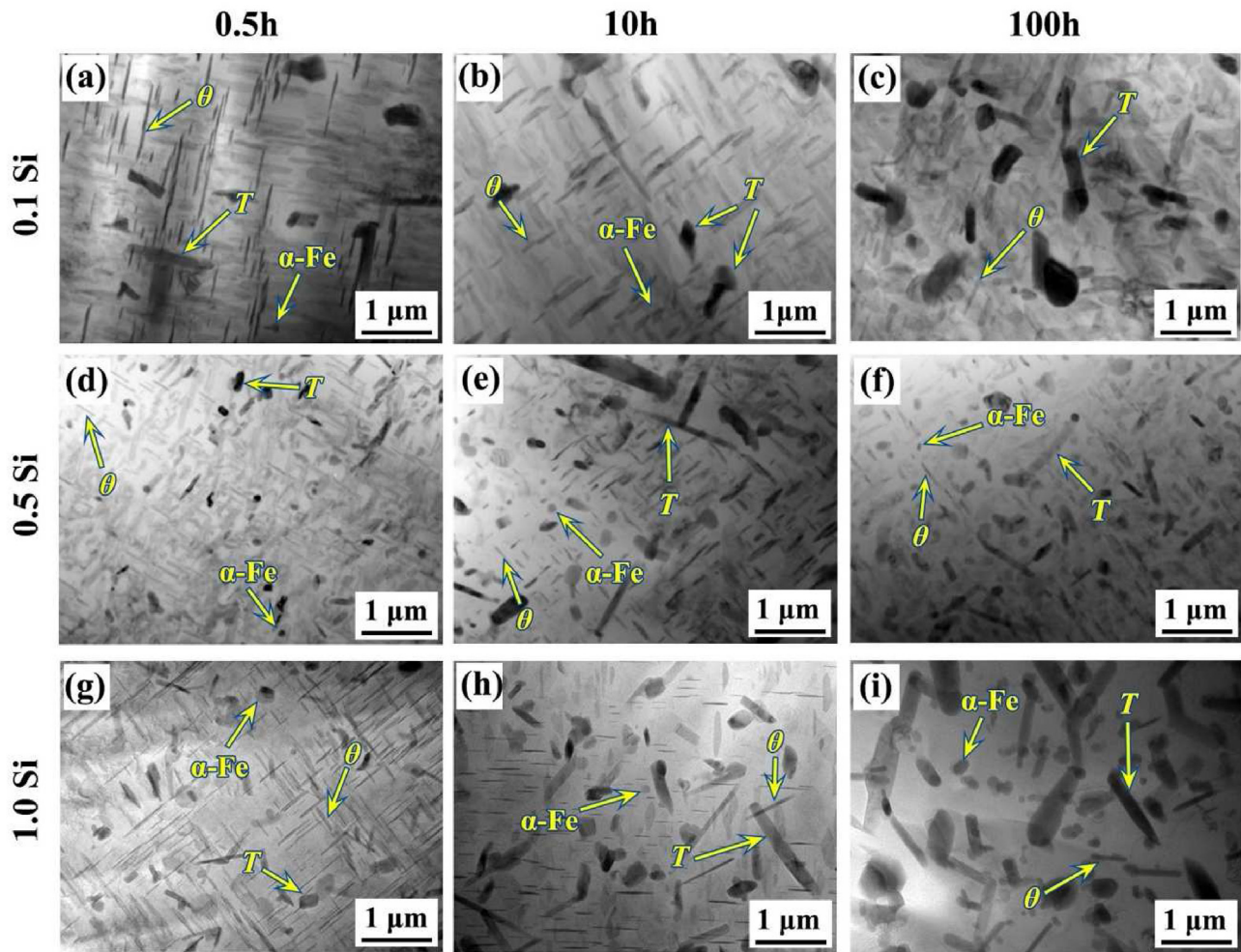


Fig. 8 – Precipitated particles of Al-6.5Cu-0.6Mn-0.5Fe alloys with different Si contents after TETT: (a) 0.1Si, 0.5 h; (b) 0.1Si, 10 h; (c) 0.1Si, 100 h; (d) 0.5Si, 0.5 h; (e) 0.5Si, 10 h; (f) 0.5Si, 100 h; (g) 1.0Si, 0.5 h; (h) 1.0Si, 10 h; (i) 1.0Si, 100 h.

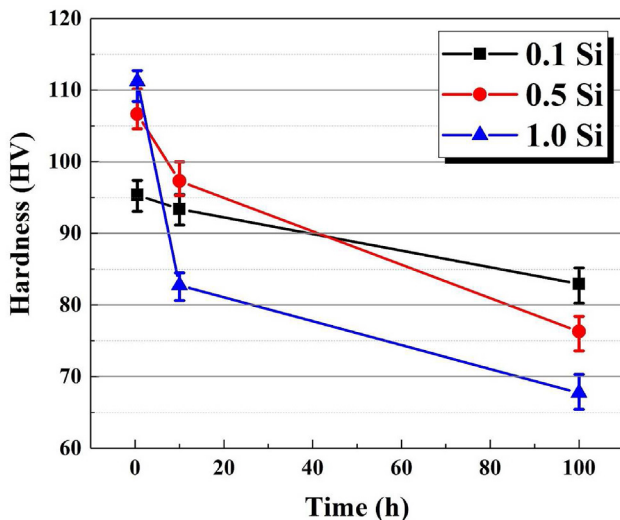


Fig. 9 – Micro-hardness of the Al-6.5Cu-0.6Mn-0.5Fe alloys with different Si contents after TETT.

heat-resistant β -Fe can prevent the sliding of the grain boundary. With increasing thermal exposure time, the ductile fracture characteristics became more apparent in the 1.0Si alloy. A large amount of dimples and Si particles appeared on the fracture surface of the 0.5Si and 1.0Si alloys when the TETT time was increased (Fig. 11d–i), which indicated that solid-state transformation of α -Fe to β -Fe became more severe. The consumption of Al_2Cu resulted from the fact that the solid-state transformation of iron-rich intermetallics worsens the reinforcement of the Al matrix, and further leads to the sliding of the Al matrix after long thermal exposure time. In Fig. 11f, some cylinder-shaped or cluster-like β -Fe were found in the 1.0Si alloy, proving the solid-state transformation of α -Fe to β -Fe.

To assess the effects of Si addition on the microstructure and fracture failure of experimental alloys, the morphologies of intermetallics on or beneath the fractured surfaces of the experimental alloys in the longitudinal direction are exhibited in Fig. 10. In the 0.1Si alloys (Fig. 12a–c), only β -Fe was observed on or beneath the fractured surfaces, indicating that the brittle β -Fe can lead to crack formation and propagation,

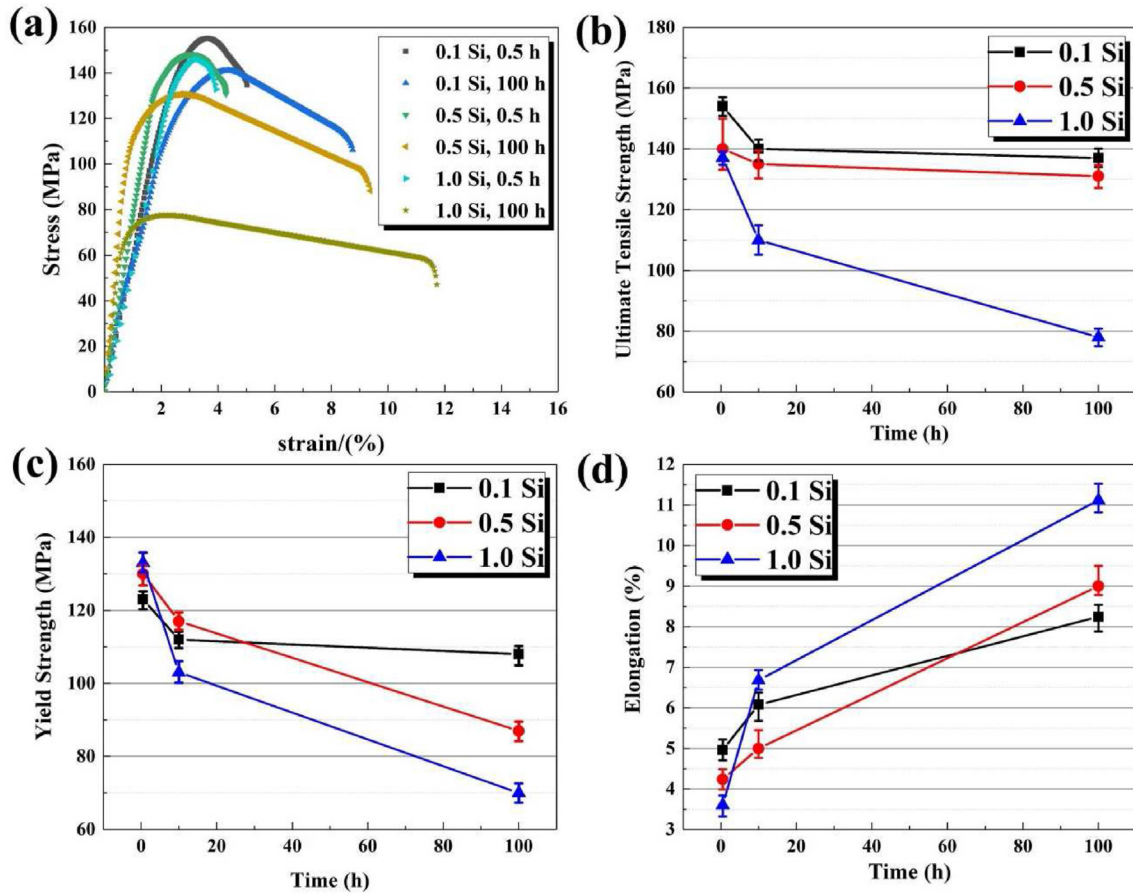


Fig. 10 – Mechanical properties of the Al-6.5Cu-0.6Mn-0.5Fe alloys with different Si contents after TETT: (a) Engineering Stress; (b) Ultimate Tensile Strength; (c) Yield Strength; (d) Ultimate Elongation.

and finally to fracture failure under tensile loading. Chinese script-like α -Fe, needle-like β -Fe, Al_2Cu , and Si particles were found on or beneath the fractured surfaces of the 0.5Si and

1.0Si alloys (Fig. 12d–i), which suggests that these particles are the main crack sources that lead to the formation and propagation of cracks during tensile loading.

Table 3 – UTS value of experimental alloys with different Si contents were compared to those of the heat resistant aluminum alloys [21–29].

Source	Alloys	Temperature (°C)	UTS (MPa)		
			0.5 h	10 h	100 h
This study	Al-6.5Cu-0.6Mn-0.5Fe-0.1Si(T7)	300	154 ± 3	140 ± 4	137 ± 3
	Al-6.5Cu-0.6Mn-0.5Fe-0.5Si(T7)	300	140 ± 3	135 ± 5	131 ± 4
	Al-6.5Cu-0.6Mn-0.5Fe-1.0Si(T7)	300	137 ± 2	110 ± 5	78 ± 3
Reference [21]	2024(T6)	315	110	85	69
Reference [21]	6061(T6)	315	85	62	41
Reference [21]	7075(T6)	315	70	62	59
Reference [21]	356.0(T6)	315	52	45	38
Reference [21]	319.0(T6)	315	90	75	66
Reference [22]	Al-6.72Si-3.90Cu-0.59Mn-0.59Fe(T6)	300	150	84	80
Reference [23]	Al-6.82Si-3.86Cu-0.58Mn-0.61Fe(T6)	300	132	77	73
Reference [24]	Al-Si-Cu-Fe-Mn(T6)	300	144	–	–
Reference [25]	Al-12Si-4Cu-2Ni-0.8 Mg(T6)	300	109.5	–	–
Reference [26]	Al-12Si-4Cu-2Ni-0.8 Mg(T6)	300	140	–	–
Reference [27]	Al-13.00Si-4Cu-0.92Mg-1.90Ni-0.16V(T6)	300	93	–	–
Reference [27]	Al-13.72Si-2Cu-1.08Mg-2.36Ni-0.20V (T6)	300	94	–	–
Reference [28]	Al-13.0Si-3.3Cu-1.3Mg-1.6Zn (T5)	315	132–145	–	–
Reference [29]	Al-Cu-1Mn-0.098Fe(T6)	300	116	–	–
Reference [29]	Al-Cu-1Mn-0.5Ni-0.097Fe(T6)	300	141	–	–

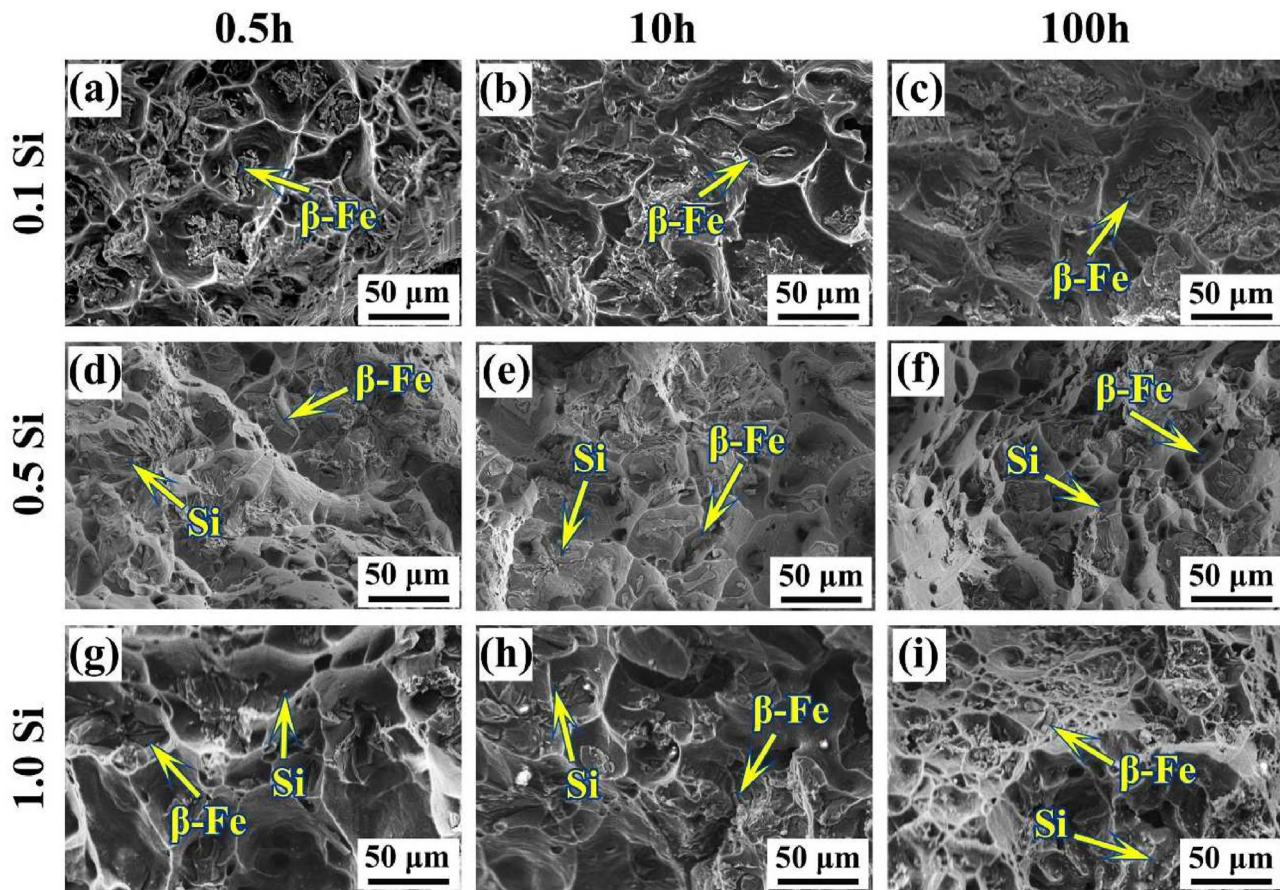


Fig. 11 – Fracture surfaces of the Al-6.5Cu-0.6Mn-0.5Fe alloys with different Si contents after TETT: (a) 0.1Si, 0.5 h; (b) 0.1Si, 10 h; (c) 0.1Si, 100 h; (d) 0.5Si, 0.5 h; (e) 0.5Si, 10 h; (f) 0.5 Si, 100 h; (g) 1.0Si, 0.5 h; (h) 1.0Si, 10 h; (i) 1.0 Si, 100 h.

4. Discussion

4.1. The α -Fe to β -Fe after TETT

Si is considered to be the most harmful impurity in cast Al–Cu–Mn alloys. On the other hand, the addition of Si has been used to promote the formation of Chinese script Fe-rich intermetallics in Al–Cu–Mn alloys with high Fe content [9–11]. Most studies have reported that the addition of Si promotes the formation of α -Fe ($\text{Al}_{15}(\text{FeMn})_3(\text{CuSi})_2$) and helps the α -Fe to remain thermodynamically stable after heat treatment [11,12]. However, it has been found that α -Fe to β -Fe occurs in Al–Cu–Mn–Fe–Si alloys after TETT. According to the solid-state phase-transformation thermodynamics of metallic materials, β -Fe is considered as the most stable iron-rich intermetallic, and α -Fe ($\text{Al}_{15}(\text{FeMn})_3(\text{CuSi})_2$) can be transformed into β -Fe, which has been reported by several studies [13,14]. According to the solid-state phase-transformation kinetics of metallic materials, a high density of dislocations results from the brittle iron-rich intermetallics within the Al matrix, and atomic matching between α -Fe and β -Fe proved the high potential nucleation locations during thermal exposure and tensile testing [30,31]. It has been proved that the α -Fe to β -Fe in Al–Cu–Mn–Fe alloys is a diffusion transformation [14]. The thermal exposure temperature and time,

the stress developed during the tensile test, and the Si content in α -Fe can affect the nucleation and growth of solid-state phase transformation [30,31]. Consequently, according to the thermodynamics and kinetics of solid-state phase transformation, this solid-state transformation of iron-rich intermetallics can occur during TETT.

4.2. Mechanical properties of the Al-6.5Cu-0.6Mn-0.5Fe alloys with different Si contents after TETT

As mentioned above, the UTS values of the experimental alloys with different Si content were higher than those of most heat-resistant Al alloys, especially the 0.1Si alloys. The high-performance mechanical properties after high-temperature thermal exposure can be attributed to the high heat resistance of secondary intermetallics and precipitated particles including the β -Fe, α -Fe, θ (Al_2Cu), T ($\text{Al}_{20}\text{Cu}_2\text{Mn}_3$), and nano-sized α -Fe phases. In general, it is an efficient method for forming thermally stable intermetallics that prevent grain boundary sliding, and enable the development of heat-resistant Al alloys. It has been reported that the iron-rich intermetallic β -Fe phases are considered to be thermally stable due to their high melting points in 2XXX and 7XXX Al alloys [16]. Certain studies have reported that the microhardness of α -Fe remains stable when the temperature is below 350 °C, which indicates that the presence of heat-

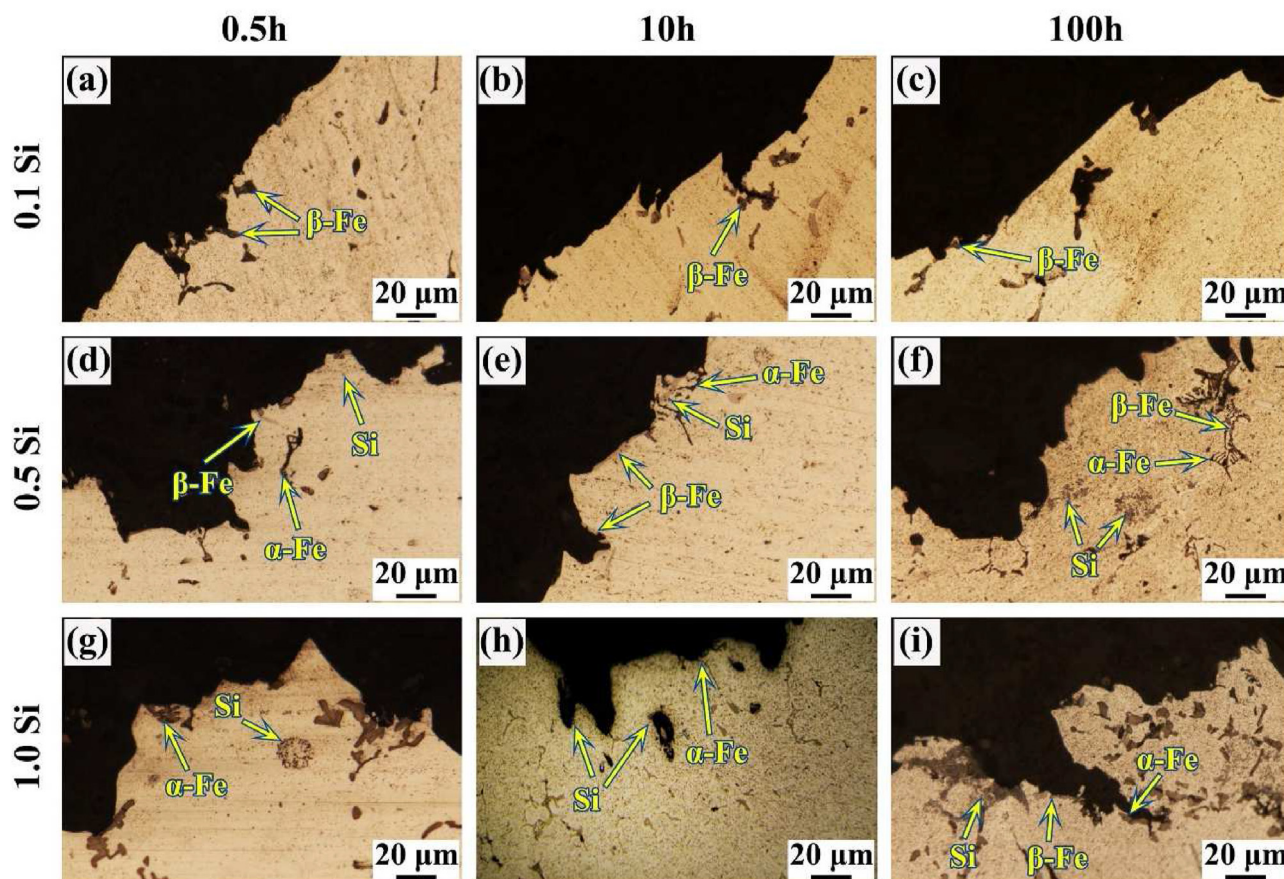


Fig. 12 – Morphologies of intermetallics on or beneath the fractured surfaces of the Al-6.5Cu-0.6Mn-0.5Fe alloys with different Si contents in the longitudinal direction: (a) 0.1Si, 0.5 h; (b) 0.1Si, 10 h; (c) 0.1Si, 100 h; (d) 0.5Si, 0.5 h; (e) 0.5Si, 10 h; (f) 0.5Si, 100 h; (g) 1.0Si, 0.5 h; (h) 1.0Si, 10 h; (i) 1.0Si, 100 h.

resistant α -Fe phases is beneficial to the improvement of the mechanical properties at elevated temperatures [22–24]. In cast Al–Si alloys, the α -Fe precipitated around the grain boundary has been found to improve the mechanical properties at elevated temperatures due to grain boundary strengthening [22–24]. As it can be observed in Fig. 14a, there were a lot of dislocations around the iron-rich intermetallics, which indicates that iron-rich intermetallics can prevent dislocation movement, further improving the high-temperature mechanical properties.

The formation of thermally stable precipitated particles in the Al matrix to prevent dislocation movement can also facilitate the development of high-strength heat-resistant Al alloys. Most studies have reported that the nano-sized α -Fe and T ($\text{Al}_{20}\text{Cu}_2\text{Mn}_3$) are thermally stable precipitated particles in Al–Si and Al–Cu alloys that are beneficial to the improvement of the mechanical properties at elevated temperatures [32,33]. In general, the θ (Al_2Cu) phases are considered to be less thermally stable and grow rapidly when the temperature is above 250 °C. Recently, some researchers found that the addition of Mn, Zr, Si, and Sc can make the θ (Al_2Cu) phases thermally stable at 300 °C, which can be attributed to the element agglomeration between the θ (Al_2Cu) phases [34,35]. In this study, it was found that the size of the θ (Al_2Cu) phases

remained nearly unchanged after TETT, indicating that the θ (Al_2Cu) phases in Al-6.5Cu-0.6Mn-0.5Fe alloys with different Si contents alloys are thermally stable. In order to reveal the source of this problem, the APT results of the 0.5Si alloy after TETT for 100 h are presented in Fig. 13. It can be found that the Mn atoms segregate at the interface between θ (Al_2Cu) phases and Al matrix, which can prevent their growth during long thermal exposure times and tensile testing conditions [35,36]. The TEM image in Fig. 14b displays the interactions between precipitated particles and dislocations in the 0.1Si alloy after TETT for 100 h. These results indicate that the θ (Al_2Cu) and T ($\text{Al}_{20}\text{Cu}_2\text{Mn}_3$) phases, as well as the α -Fe dispersoids can efficiently prevent dislocation motion and consume strain energy during tensile deformation, even after thermal exposure for 100 h.

4.3. Effect of Si content on the mechanical properties of Al-6.5Cu-0.6Mn-0.5Fe alloys after TETT

Under all thermal exposure times (0.5 h, 10 h, or 100 h), the UTS decreased slightly when the Si content was increased from 0.1% to 0.5%, and then decreased dramatically when the Si content was increased to 1.0%. The decrease of UTS with increasing Si content can be attributed to the solid-state phase

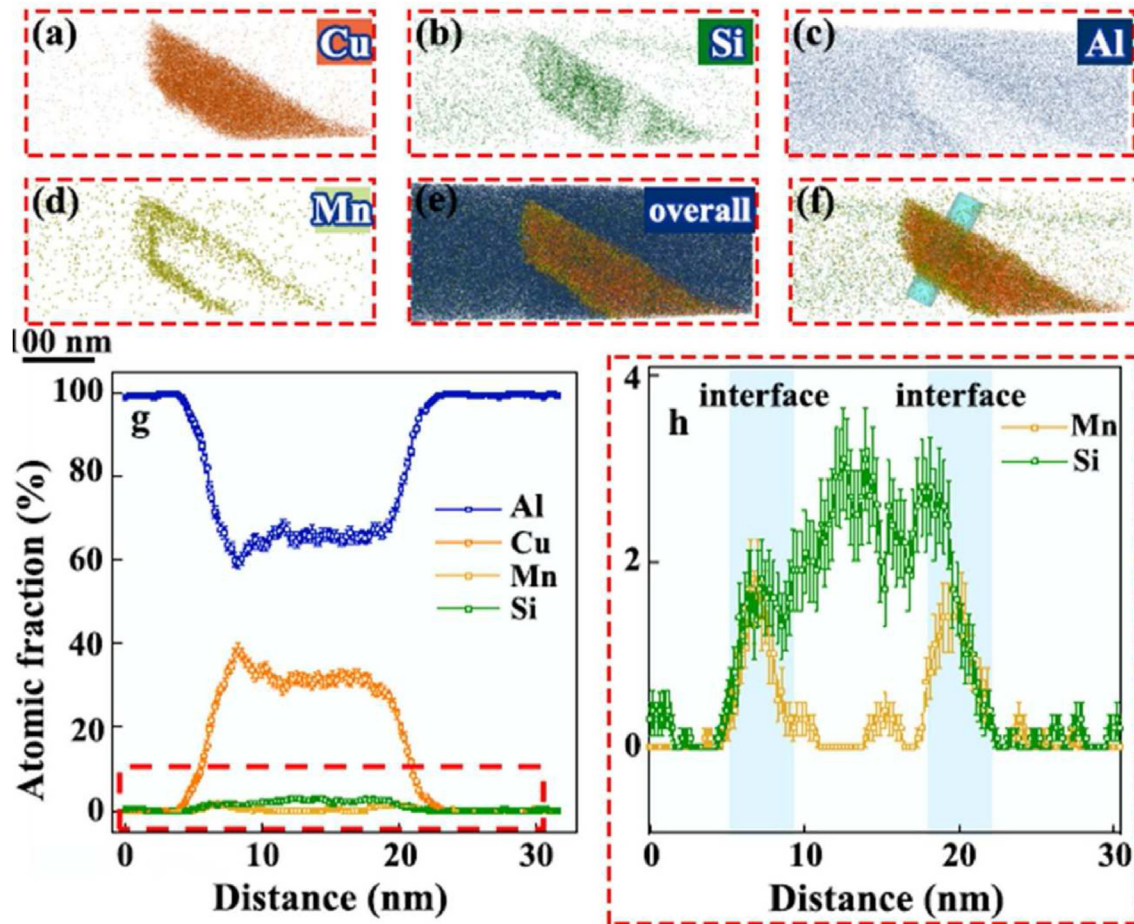


Fig. 13 – APT reconstruction; (a–e) elements distribution; (f) the cylinder position for concentration profile; (g) 1-dimensional elements concentration profile; (h) magifaion of Mn and Si elements line distribution.

transformation of iron-rich intermetallics after TETT. The solid-state phase transformation of iron-rich intermetallics resulted in the increase of needle-like Fe-rich phases and Si

particles, the agglomeration of secondary intermetallics, as well as the consumption of Al_2Cu phases, which are harmful to alloys with high Si content. A number of studies have reported

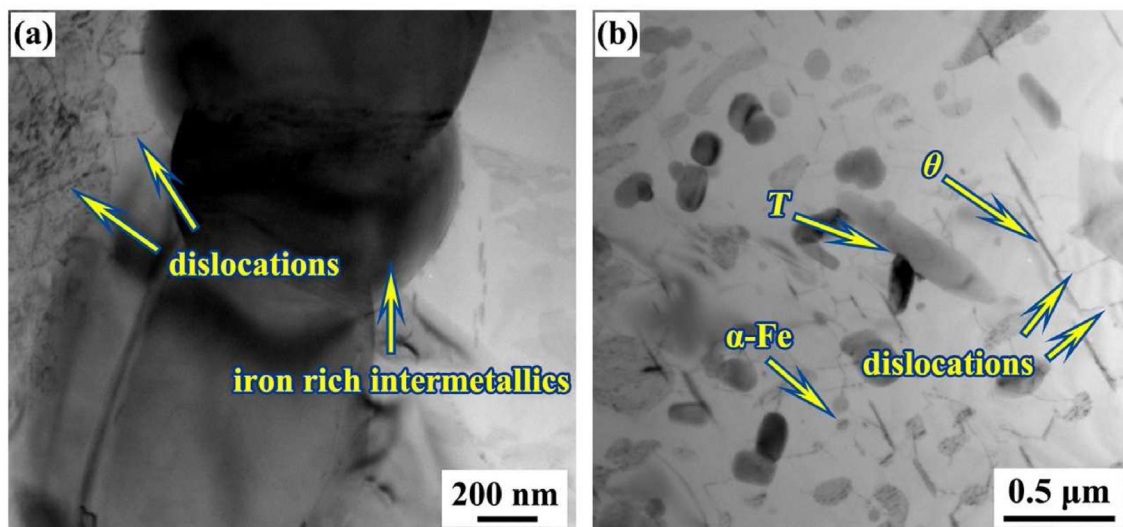


Fig. 14 – TEM image of interactions between iron-rich intermetallics, precipitates and dislocations in 0.1Si alloy after TETT for 100 h.

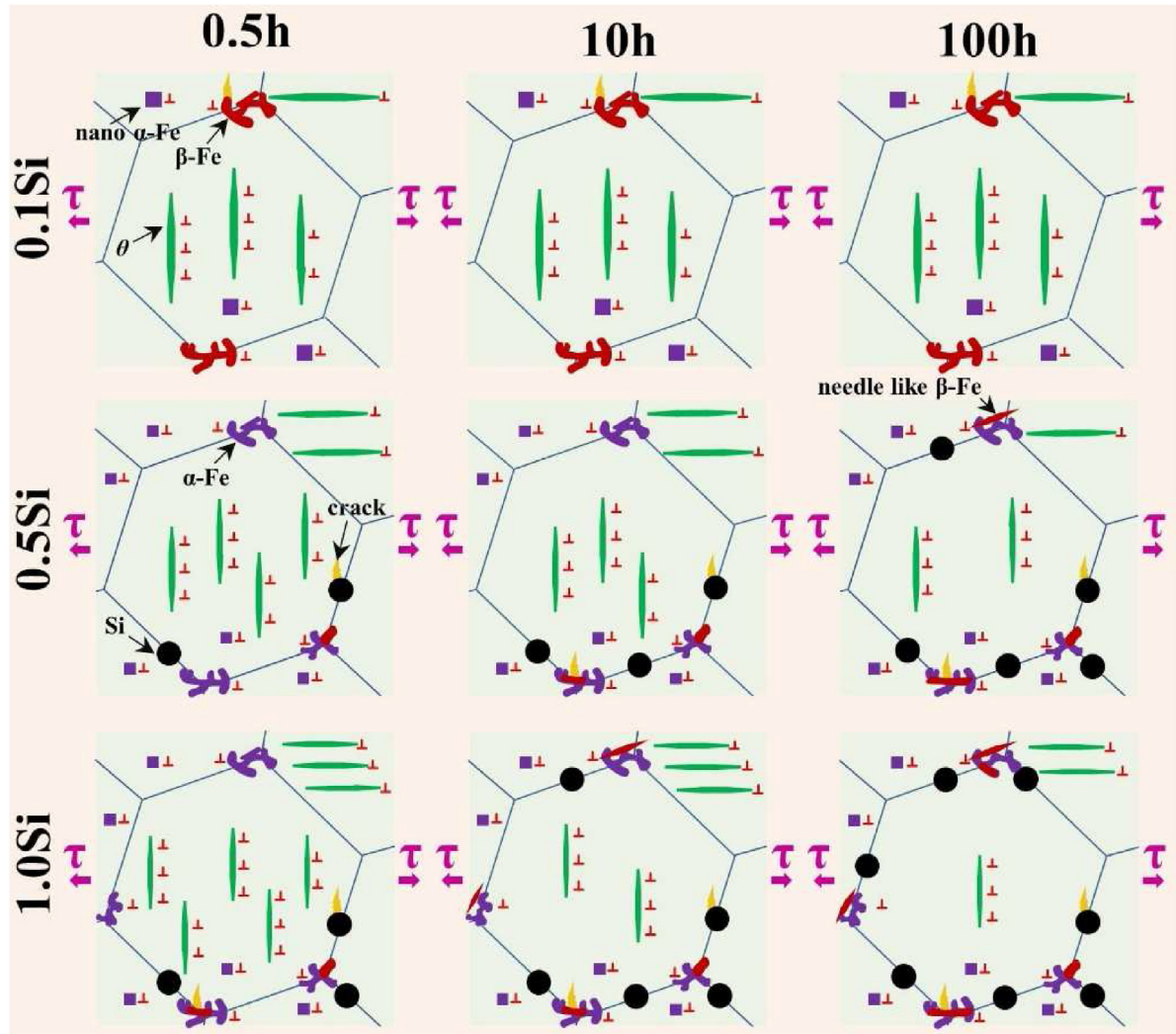


Fig. 15 – Evolution of secondary intermetallics and the high-temperature fracture of Al–Cu–Mn–Fe–Si alloys after TETT for different times.

that the needle-like Fe-rich phases and Si particles can deteriorate the UTS [12,22–24]. According to Fig. 5, the α -Fe to β -Fe intensifies with increasing thermal exposure time and Si content, which may have caused the sharp decrease of the UTS.

When the TETT time was 0.5 h, the YS increased slightly with the increase of Si content. When TETT for 100 h, the YS decreased with the Si content, especially in 1.0Si alloy. The increase of the YS with Si addition and short thermal exposure time can be attributed to the refinement of the θ (Al_2Cu) and α -Fe phases in the Al matrix, as well as to the increase of their contents due to the addition of Si. However, when the thermal exposure time was increased to 100 h, the α -Fe to β -Fe as well as the consumption of Al_2Cu intensified, leading to the further decrease of the YS.

When the TETT time was 0.5 h, the EL decreased slightly with the increase of Si content. When the TETT was 100 h, the EL increased with the Si content, especially in 1.0Si alloy. The decrease of EL can be attributed to the increase of the iron-rich intermetallics with increasing Si content. On the other hand, the increase of EL after long thermal exposure can be

attributed to the α -Fe to β -Fe. In general, the solid-state transformation decreases the Al_2Cu phases in the Al matrix, causing the sliding of the Al matrix, and further increasing the EL.

Fig. 15 unfolds the evolution of secondary intermetallics and the high-temperature fracture of Al–Cu–Mn–Fe–Si alloys after TETT for different times based on the above results. In this study, the Si addition is detrimental to the high-temperature mechanical properties of Al-6.5Cu-0.6Mn-0.5Fe alloys, which is attributed to the α -Fe to β -Fe. It is very important to obtain heat-stable phases in order to develop heat-resistant Al alloys. As a result, the presence of unstable α -Fe makes the development of heat-resistant Al–Cu alloys with high Fe and Si content a great challenge. This result implies that Si is not suitable for modifying the iron-rich intermetallics in Al–Cu–Mn–Fe alloys used as important light heat-resistant structural components. Nevertheless, the UTS values of the Al-6.5Cu-0.6Mn-0.5Fe with high Si content were higher than or close to those of commercial Al alloys, which indicates that these alloys can be used as unimportant heat-

resistant structural parts operating under short-time high-temperature conditions in civil applications.

5. Conclusions

- (1) A solid-state transformation of iron-rich intermetallics from α -Fe to β -Fe occurred in the Al-6.5Cu-0.6Mn-0.5Fe alloys with high Si content after thermal exposure followed by tensile testing at 300 °C. This solid-state transformation can be expressed as follows: α -Fe ($(Al_{15}(FeMn)_3(CuSi)_2) + 4 Al_2Cu \rightarrow 3 \beta$ -Fe (Al_7Cu_2 -FeMn) + 2 Si + 2 α (Al)). With the increase of the thermal exposure time and Si content, the solid-state transformation from α -Fe to β -Fe intensifies, and the newly formed Si particles agglomerate with Al_2Cu phases.
- (2) The addition of Si in Al-6.5Cu-0.6Mn-0.5Fe alloys promotes the formation of nano-sized θ (Al_2Cu) and α -Fe phases in the Al matrix and refines the precipitated particles drastically.
- (3) The UTS values of the Al-6.5Cu-0.6Mn-0.5Fe-0.1Si alloy after thermal exposure for 0.5 h, 10 h, and 100 h, followed by tensile testing at 300 °C were 154 MPa, 140 MPa, and 137 MPa, respectively, which are higher than those of most heat-resistant Al alloys. The high-performance mechanical properties at elevated temperatures can be attributed to the high heat resistance of secondary intermetallics and precipitated particles, including the θ (Al_2Cu), β -Fe, α -Fe, T ($Al_{20}Cu_2Mn_3$), and nano-sized α -Fe phases.
- (4) The UTS values of the Al-6.5Cu-0.6Mn-0.5Fe-0.5Si alloy after thermal exposure for 0.5 h, 10 h, and 100 h, followed by tensile testing at 300 °C were 140 MPa, 135 MPa, and 131 MPa, respectively, which are also higher than or close to those of most heat-resistant Al alloys. These alloys with high Fe and Si contents can be used as unimportant heat-resistant structural parts operating under short-time high-temperature conditions in civil applications, which provides theoretical basis and technical support for promoting the efficient utilization of recycled Al alloys.
- (5) The addition of Si deteriorates the strength of Al-6.5Cu-0.6Mn-0.5Fe alloys after long thermal exposure. This can be attributed to the solid phase transformation of iron-rich intermetallics from α -Fe to β -Fe, which results in the increase of needle-like Fe-rich phases and Si particles, the agglomeration of secondary intermetallics, and the consumption of Al_2Cu phases. This result implies that Si is not suitable for modifying the iron-rich intermetallics in Al–Cu–Mn–Fe alloys used as important light heat-resistant structural components in military and aerospace industries.

Declaration of competing interest

The authors declare that they have no known competing financial interests or personal relationships that could have appeared to influence the work reported in this paper.

Acknowledgments

This work was supported by the National Natural Science Foundation of China [52265043]; Science and Technology Plan, Guizhou Province, China [ZK2021(267)]; Technology Achievements Application and Industrialization project, Guizhou Province, China [2021(067)]; Cultivation Project of Guizhou University [2019(23)]; Science and Technology Planning Project of Guiyang in China (No. 2021.1–4); and the National Key Research and Development Program Science and Technology for Economy 2020 Key Special Project (No. SQ2020YFF0421630). This work was partly carried out with the support of the Karlsruhe Nano Micro Facility (KNMF, www.knmf.kit.edu), a Helmholtz Research Infrastructure at Karlsruhe Institute of Technology.

REFERENCES

- [1] Rakhmonov JU, Bahl S, Shyam A, Dunand DC. Cavitation-resistant intergranular precipitates enhance creep performance of θ' -strengthened Al-Cu based alloys. *Acta Mater* 2022;228:117788. <https://doi.org/10.1016/j.actamat.2022.117788>.
- [2] Fan JC, Yang BW, Wang Y, Gao MQ, Guan RG. Enhancing the tensile strength and heat resistance induced by high-density Ω phases in an Al-Cu-Mg-Ag alloy. *J Mater Res Technol* 2022;18:3347–57. <https://doi.org/10.1016/j.jmrt.2022.04.015>.
- [3] Zhao YL, Song DF, Wang HW, Li XX, Chen LJ, Sun ZZ, et al. Revealing the nucleation and growth mechanisms of Fe-rich phases in Al-Cu-Fe (-Si) alloys under the influence of Al-Ti-B. *Intermetallics* 2022;146:107584. <https://doi.org/10.1016/j.intermet.2022.107584>.
- [4] Association A. *Designations and chemical composition limits for aluminum alloys in the form of castings and ingot*. Arlington, VA, USA: The Aluminum Association; 2006.
- [5] Lin R, Liu B, Zhang JJ, Zhang SG. Microstructure evolution and properties of 7075 aluminum alloy recycled from scrap aircraft aluminum alloys. *J Mater Res Technol* 2022;19:354–67. <https://doi.org/10.1016/j.jmrt.2022.05.011>.
- [6] Green JAS. *Aluminum recycling and processing for energy conservation and sustainability*. ASM International; 2007.
- [7] Qiu Y, Zheng KH, Li XT, Luo YJ, Xia P, Liu MY, et al. Processing map of 2219 Al alloy prepared by internal electromagnetic stirring direct chill casting. *J Mater Res Technol* 2022;18:2885–95. <https://doi.org/10.1016/j.jmrt.2022.03.177>.
- [8] Schuster M, De Luca A, Widmer R, Maeder X, Leinenbach C. Processability, microstructure and precipitation of a Zr-modified 2618 aluminium alloy fabricated by Laser Powder Bed Fusion. *J Alloys Compd* 2022;913:165346. <https://doi.org/10.1016/j.jallcom.2022.165346>.
- [9] Kanga HK, Larouche D, Bourmane M, Rahem A. Mechanical properties of aluminium–copper B206 alloys with iron and silicon additions. *Int J Cast Metals Res* 2012;25(1):15–25. <https://doi.org/10.1179/1743133610Y.0000000012>.
- [10] Liu K, Cao X, Chen XG. Tensile properties of Al-Cu 206 cast alloys with various iron contents. *Metall Mater Trans* 2014;45(5):2498–507. <https://doi.org/10.1007/s11661-014-2207-3>.
- [11] Zhao YL, Zhang WW, Yang C, Zhang DT, Wang Z. Effect of Si on Fe-rich intermetallic formation and mechanical properties of heat-treated Al-Cu-Mn-Fe alloys. *J Mater Res* 2018;33(8):898–911. <https://doi.org/10.1557/jmr.2017.441>.

- [12] Xu R, Lin B, Li HY, Xiao HQ, Zhao YL, Zhang WW. Microstructure evolution and mechanical properties of Al-6.5 Cu-0.6 Mn-0.5 Fe alloys with different Si additions. *Trans Nonferrous Metals Soc China* 2019;29(8):1583–91. [https://doi.org/10.1016/S1003-6326\(19\)65065-X](https://doi.org/10.1016/S1003-6326(19)65065-X).
- [13] Lin B, Zhang WW, Zhao YL, Li YY. Solid-state transformation of Fe-rich intermetallic phases in Al-5.0 Cu-0.6 Mn squeeze cast alloy with variable Fe contents during solution heat treatment. *Mater Char* 2015;104:124–31. <https://doi.org/10.1016/j.matchar.2015.03.035>.
- [14] Liu K, Cao X, Chen XG. Solid-state transformation of iron-rich intermetallic phases in Al-Cu 206 cast alloys during solution heat treatment. *Metall Mater Trans* 2013;44(8):3494–503. <https://doi.org/10.1007/s11661-013-1726-7>.
- [15] Lin B, Zhang WW, Lou ZH, Zhang DT, Li YY. Comparative study on microstructures and mechanical properties of the heat-treated Al-5.0 Cu-0.6 Mn-xFe alloys prepared by gravity die casting and squeeze casting. *Mater Des* 2014;59:10–8. <https://doi.org/10.1016/j.matdes.2014.02.012>.
- [16] Chen CL, Thomson RC. Study on thermal expansion of intermetallics in multicomponent Al-Si alloys by high temperature X-ray diffraction. *Intermetallics* 2010;18(9):1750–7. <https://doi.org/10.1016/j.intermet.2010.05.015>.
- [17] Li JY, Lü SL, Wu SS, Zhao DJ, Guo W. Micro-mechanism of simultaneous improvement of strength and ductility of squeeze-cast Al-Cu alloy. *Mater Sci Eng, A* 2022;833:142538. <https://doi.org/10.1016/j.msea.2021.142538>.
- [18] Dar SM, Liao HC, Xu A. Quasicrystalline phases in conventionally cast Fe-containing Al-Cu-Mn alloys and its evolution during the annealing at 530°C. *Mater Lett* 2021;301:130322. <https://doi.org/10.1016/j.matlet.2021.130322>.
- [19] Majid SAE, Bamberger M, Katsman A. Microstructure and phase evolution in A201 alloys with additions of silicon. In: *Light metals 2016*. Cham: Springer; 2016. p. 127–30.
- [20] Mitlin Jr Jwm D, Radmilovic V. Catalyzed precipitation in Al-Cu-Si. *Metall Mater Trans* 2000;31(11):2697–711. <https://doi.org/10.1007/BF02830329>.
- [21] Kaufman JG. *Properties of aluminum alloys: tensile, creep, and fatigue data at high and low temperatures*. ASM international; 1999.
- [22] Lin B, Fan T, Li HY, Zhao YL, Zhang WW, Liu K. Microstructure and high temperature tensile properties of Al-Si-Cu-Mn-Fe alloys prepared by semi-solid thixoforming. *Trans Nonferrous Metals Soc China* 2021;31(8):2232–49. [https://doi.org/10.1016/S1003-6326\(21\)65651-0](https://doi.org/10.1016/S1003-6326(21)65651-0).
- [23] Lin B, Li HY, Xu R, Zhao YL, Xiao HQ, Tang ZQ, Li SB. Thermal exposure of Al-Si-Cu-Mn-Fe alloys and its contribution to high temperature mechanical properties. *J Mater Res Technol* 2020;9(2):1856–65. <https://doi.org/10.1016/j.jmrt.2019.12.018>.
- [24] Wang ER, Hui XD, Chen GL. Eutectic Al-Si-Cu-Fe-Mn alloys with enhanced mechanical properties at room and elevated temperature. *Mater Des* 2011;32(8–9):4333–40. <https://doi.org/10.1016/j.matdes.2011.04.005>.
- [25] Han L, Sui YD, Wang QD, Qang K, Jiang YH. Effects of Nd on microstructure and mechanical properties of cast Al-Si-Cu-Ni-Mg piston alloys. *J Alloys Compd* 2017;695:1566–72. <https://doi.org/10.1016/j.jallcom.2016.10.300>.
- [26] Sui YD, Ji DP, Han LN, Wang QD. Characterization of the aging precipitates of Al-12Si-4Cu-2Ni-0.8 Mg-0.2 Gd piston alloy. *JOM (J Occup Med)* 2019;71(1):366–72. <https://doi.org/10.1007/s11837-018-3080-0>.
- [27] Aikawa T, Ishikawa A, Hara S. Aluminum alloy for internal-combustion piston, and aluminum alloy piston. U.S. Patent 5 1999;996(471):12. 7.
- [28] Takasaki N, Yoshimura Y. Heat resistant Al die cast material. U.S. Patent 6 2004;706(242):3–16.
- [29] Chen JL, Liao HC, Wu YN, Li HL. Contributions to high temperature strengthening from three types of heat-resistant phases formed during solidification, solution treatment and ageing treatment of Al-Cu-Mn-Ni alloys respectively. *Mater Sci Eng, A* 2020;772:138819. <https://doi.org/10.1016/j.msea.2019.138819>.
- [30] Alexander DTL, Greer AL. Solid-state intermetallic phase transformations in 3XXX aluminium alloys. *Acta Mater* 2002;50(10):2571–83. [https://doi.org/10.1016/S1359-6454\(02\)00085-X](https://doi.org/10.1016/S1359-6454(02)00085-X).
- [31] Carter CB, Norton MG. *Solid-state phase transformations and reactions*. In: *Ceramic materials*. New York, NY: Springer; 2013. p. 457–75.
- [32] Liao HC, Tang YY, Sui XJ, Li GJ, Hu YY, Dixit US, et al. Dispersoid particles precipitated during the solutionizing course of Al-12 wt% Si-4 wt% Cu-1.2 wt% Mn alloy and their influence on high temperature strength. *Mater Sci Eng, A* 2017;699:201–9. <https://doi.org/10.1016/j.msea.2017.04.091>.
- [33] Liu K, Chen XG. Improvement in elevated-temperature properties of Al-13% Si piston alloys by dispersoid strengthening via Mn addition. *J Mater Res* 2018;33(20):3430–8. <https://doi.org/10.1557/jmr.2018.117>.
- [34] Gao YH, Cao LF, Kuang J, Song H, Liu G, Zhang JY, et al. Solute repositioning to tune the multiple microalloying effects in an Al-Cu alloy with minor Sc, Fe and Si addition. *Mater Sci Eng, A* 2021;803:140509. <https://doi.org/10.1016/j.msea.2020.140509>.
- [35] Sun TT, Geng JW, Bian ZY, Wu Y, Wang ML, Chen D, et al. Enhanced thermal stability and mechanical properties of high-temperature resistant Al-Cu alloy with Zr and Mn micro-alloying. *Trans Nonferrous Metals Soc China* 2022;32(1):64–78. [https://doi.org/10.1016/S1003-6326\(21\)65778-3](https://doi.org/10.1016/S1003-6326(21)65778-3).
- [36] Shower P, Poplawsky J, Bahl S, Shyam A. The role of Si in determining the stability of the θ' precipitate in Al-Cu-Mn-Zr alloys. *J Alloys Compd* 2021;862:158152. <https://doi.org/10.1016/j.jallcom.2020.158152>.